

Crack Analysis in Piezoelectric Solids with Energetically Consistent Boundary Conditions by the MLPG

J. Sladek¹, V. Sladek¹, Ch. Zhang² and M. Wünsche²

Abstract: A meshless method based on the local Petrov-Galerkin approach is proposed to solve initial-boundary value crack problems of piezoelectric solids with nonlinear electrical boundary conditions on crack faces. Homogeneous and continuously varying material properties of the piezoelectric solid are considered. Stationary governing equations for electrical fields and the elastodynamic equations with an inertial term for mechanical 2-D fields are considered. Nodal points are spread on the analyzed domain, and each node is surrounded by a small circle for simplicity. The spatial variation of displacements and electric potential are approximated by the Moving Least-Squares (MLS) scheme. After performing the spatial integrations, one obtains a system of ordinary differential equations for certain nodal unknowns. That system is solved numerically by the Houbolt finite-difference scheme as a time-stepping method. An iterative solution algorithm is developed to consider the energetically consistent crack-face boundary conditions. The accuracy of the present method for computing the stress intensity factors (SIF) and electrical displacement intensity factor (EDIF) are discussed by comparison with available analytical or numerical solutions.

Keywords: Meshless local Petrov-Galerkin method (MLPG), Moving least-squares (MLS) interpolation, piezoelectric solids, functionally graded materials, intensity factors, dynamic loading

1 Introduction

Modern smart structures, made of piezoelectric materials, offer certain potential performance advantages over conventional ones, due to their capability of converting the mechanical energy to electric one and vice versa. They are extensively utilized as transducers, sensors and actuators in many engineering fields. Piezo-

¹ Institute of Construction and Architecture, Slovak Academy of Sciences, 84503 Bratislava, Slovakia

² Department of Civil Engineering, University of Siegen, D-57068 Siegen, Germany

electric ceramics are very brittle and susceptible to fracture during service. To prevent failure, the fracture behaviour of these materials must be well understood. Recently, the study of singular stress and electric fields in cracked piezoelectric materials has attracted the attention of many researchers. Pak (1990) obtained the closed form solutions for an infinite piezoelectric medium under anti-plane loading by using a complex variable approach. Later, Park and Sun (1995) obtained closed form solutions for all three fracture modes for a crack in an infinite piezoelectric medium. They investigated the effect of the electric field on the fracture of piezoelectric ceramics. A review and other literature sources on the fracture of piezoelectric materials can be found in McMeeking (1999) and Kuna (2006).

Functionally graded materials (FGMs) have demonstrated that they have a potential to reduce the stress concentration and increase the fracture toughness [Suresh and Mortensen (1998); Paulino et al. (2003)]. Consequently, the concept of FGMs can be extended to the piezoelectricity to obtain piezoelectric materials with high strength, high toughness, low thermal expansion coefficient and low dielectric constant. Devices such as actuators based on functionally graded piezoelectric materials (FGPMs) were given by Zhu et al. (1995, 1999). The fracture of FGPMs under a thermal load has been studied by Wang and Noda (2001). An anti-plane crack problem is described by relatively simpler governing equations than for in-plane problems [Li and Weng (2002)]. Recently, the in-plane crack problem in FGPMs has been analyzed by Chen et al. (2003) and Ueda (2003).

The electric boundary condition on the piezoelectric crack-surfaces comes in different degrees of shielding the electric induction defined by the electric permeability. The permeable crack does not shield the electric induction. The second extreme case, the impermeable crack shields the electric induction completely. If the crack is closed, the permeable boundary conditions are correct, while the impermeable conditions are every time incorrect, since the assumption of the vanishing permittivity of the crack medium is not applicable. The permittivity of the vacuum is a finite value of $8.854 \cdot 10^{-12} C/Vm$. If the crack opening displacement is extremely small (at low mechanical load), the permeable boundary condition may provide a good approximation despite its inconsistency [Denda (2008)]. The semi-permeable boundary conditions proposed by Hao and Shen (1994) consider finite value of the permittivity and crack opening displacement. The electrical field in the crack gap is approximated as the potential drop divided by the crack opening displacement. This model is leading to a problem with nonlinear boundary conditions. It is assumed here that the crack-faces are traction-free like in the previous two models. Recently, McMeeking (2004) investigated the energy release rates for a Griffith crack for all three models and found that there exists a discrepancy between the total energy release rate from the entire system and the crack-tip energy release rate.

Landis (2004) considered energetically consistent boundary conditions on crack-faces, where additional closing traction is added to well known semi-permeable boundary conditions. He showed that his modified crack conditions are leading to consistency of total and crack tip energy release rates.

The solution of the boundary value problems for continuously nonhomogeneous piezoelectric solids requires advanced numerical methods due to the high mathematical complexity. The governing equations are more complicated than in a homogeneous counterpart and the electric and mechanical fields are coupled each other. Therefore, a variety of different crack problems in piezoelectric medium has been studied only in homogeneous or multi-layered bodies. Modern computational methods like the finite element method (FEM) [Gruebner et al. (2003); Govorukha and Kamlah (2004); Enderlein et al. (2005), Kuna (1998, 2006)] and the boundary element method (BEM) [Pan (1999); Davi and Milazzo (2001); Gross et al. (2005); Garcia-Sanchez et al. (2005, 2007); Sheng and Sze (2006); Denda (2008); Wünsche et al. (2010)] have to be applied for general crack analyses in piezoelectric homogeneous solids. In spite of the great success on these effective numerical tools for the solution of boundary value problems in piezoelectric solids, there is still a growing interest in the development of new advanced methods. In recent years, meshless formulations are becoming popular due to their high adaptivity and low costs to prepare input and output data for numerical analyses. A variety of meshless methods has been proposed so far and some of them also applied to piezoelectric problems [Ohs and Aluru (2001); Liu et al. (2002)]. They can be derived either from a weak-form formulation on the global domain or a set of local subdomains. In the global formulation, background cells are required for the integration of the weak-form. In the methods based on the local weak-form formulation no background cells are required and therefore they are often referred to as truly meshless methods. The meshless local Petrov-Galerkin (MLPG) method is a fundamental base for the derivation of many meshless formulations, since trial and test functions can be chosen from different functional spaces. Recently, the MLPG method with a Heaviside step function as the test functions [Atluri et al. (2003); Atluri (2004); Sladek et al. (2004)] has been applied to solve two-dimensional (2D) homogeneous piezoelectric problems by the authors [Sladek et al. (2006)] and later also to crack problems in continuously nonhomogeneous medium [Sladek et al. (2007a)]. In previous MLPG applications to crack problems only impermeable or permeable crack conditions are considered.

In the present paper, the MLPG is extended to crack analysis in continuously nonhomogeneous piezoelectric solids with energetically consistent crack-face boundary conditions. The electrical displacements on both crack-surfaces are proportional to the ratio of the potential jump and the distance of the crack-surfaces (crack-

opening-displacement). Similarly, the traction on the crack-faces is proportional to the quadratic value of the same ratio. Since the crack-opening-displacement is dependent on the value of the electrical displacement, the problem has to be solved iteratively. The coupled governing partial differential equations are satisfied in a weak-form on small fictitious subdomains. Nodal points are introduced and spread on the analyzed domain and each node is surrounded by a small circle for simplicity, but without loss of generality. If the shape of subdomains has a simple form, numerical integrations over them can be easily carried out. The integral equations have a very simple nonsingular form. The spatial variations of the displacements and the electric potential are approximated by the Moving Least-Squares (MLS) scheme [Belytschko et al. (1996); Zhu et al. (1998)]. After performing the spatial MLS approximation, a system of ordinary differential equations for certain nodal unknowns is obtained. Then, the system of the ordinary differential equations of the second order resulting from the equations of motion is solved by the Houbolt finite-difference scheme (Houbolt 1950) as a time-stepping method. Influence of energetically consistent, semi-permeable, permeable and impermeable crack-face boundary conditions is investigated in numerical examples.

2 Local integral equations for 2D problems

The governing equations for continuously nonhomogeneous piezoelectric solids are given by the equations of motion for the mechanical displacements and by the first Maxwell equation for the vector of electric displacements [Parton and Kudryavtsev (1988)]

$$\sigma_{ij,j} + X_i = \rho \ddot{u}_i, \quad (1)$$

$$D_{j,j} - R = 0, \quad (2)$$

where \ddot{u}_i , σ_{ij} , D_i , X_i , R and ρ denote the acceleration, stress tensor, electric displacements, body force vector, volume density of free charges and mass density, respectively.

The constitutive relations represent the coupling of the mechanical and the electrical fields. They can be obtained as derivatives of the electric enthalpy density $W = W(\varepsilon_{ij}, E_i, x_i)$ [Parton and Kudryavtsev (1988)] in the following manner

$$W(\varepsilon_{ij}, E_i, \mathbf{x}) = \frac{1}{2} c_{ijkl}(\mathbf{x}) \varepsilon_{ij}(\mathbf{x}) \varepsilon_{kl}(\mathbf{x}) - e_{ikl}(\mathbf{x}) E_i(\mathbf{x}) \varepsilon_{kl}(\mathbf{x}) - \frac{1}{2} h_{ij}(\mathbf{x}) E_i(\mathbf{x}) E_j(\mathbf{x}), \quad (3)$$

$$\sigma_{ij}(\mathbf{x}) = \frac{\partial W}{\partial \varepsilon_{ij}} = c_{ijkl}(\mathbf{x}) \varepsilon_{kl}(\mathbf{x}) - e_{kij}(\mathbf{x}) E_k(\mathbf{x}), \quad (4)$$

$$D_j(\mathbf{x}) = -\frac{\partial W}{\partial E_j} = e_{jkl}(\mathbf{x})\varepsilon_{kl}(\mathbf{x}) + h_{jk}(\mathbf{x})E_k(\mathbf{x}), \quad (5)$$

where $c_{ijkl}(\mathbf{x})$, $e_{jkl}(\mathbf{x})$ and $h_{jk}(\mathbf{x})$ are the elastic, piezoelectric and dielectric material tensors in a continuously nonhomogeneous piezoelectric medium, respectively. The strain tensor ε_{ij} and the electric field vector E_j are related to the displacements u_i and the electric potential ψ , respectively, as

$$\varepsilon_{ij} = \frac{1}{2}(u_{i,j} + u_{j,i}), \quad (6)$$

$$E_j = -\psi_{,j}. \quad (7)$$

In the case of some crystal symmetries, one can formulate also the plane-deformation problems (Patron and Kudryavtsev 1988). For instance, in the crystals of hexagonal symmetry (class $6mm$) with x_3 being the 6-order symmetry axis and assuming $u_2 = 0$ as well as the independence of the field quantities on x_2 , i.e. $(\cdot)_{,2} = 0$, we have $\varepsilon_{22} = \varepsilon_{23} = \varepsilon_{12} = E_2 = 0$. Then, the constitutive equations (4) and (5) are reduced to the following forms

$$\begin{aligned} \begin{bmatrix} \sigma_{11} \\ \sigma_{33} \\ \sigma_{13} \end{bmatrix} &= \begin{bmatrix} c_{11} & c_{13} & 0 \\ c_{13} & c_{33} & 0 \\ 0 & 0 & c_{44} \end{bmatrix} \begin{bmatrix} \varepsilon_{11} \\ \varepsilon_{33} \\ 2\varepsilon_{13} \end{bmatrix} - \begin{bmatrix} 0 & e_{31} \\ 0 & e_{33} \\ e_{15} & 0 \end{bmatrix} \begin{bmatrix} E_1 \\ E_3 \end{bmatrix} \\ &= \mathbf{C}(\mathbf{x}) \begin{bmatrix} \varepsilon_{11} \\ \varepsilon_{33} \\ 2\varepsilon_{13} \end{bmatrix} - \mathbf{L}(\mathbf{x}) \begin{bmatrix} E_1 \\ E_3 \end{bmatrix}, \quad (8) \end{aligned}$$

$$\begin{aligned} \begin{bmatrix} D_1 \\ D_3 \end{bmatrix} &= \begin{bmatrix} 0 & 0 & e_{15} \\ e_{31} & e_{33} & 0 \end{bmatrix} \begin{bmatrix} \varepsilon_{11} \\ \varepsilon_{33} \\ 2\varepsilon_{13} \end{bmatrix} + \begin{bmatrix} h_{11} & 0 \\ 0 & h_{33} \end{bmatrix} \begin{bmatrix} E_1 \\ E_3 \end{bmatrix} \\ &= \mathbf{G}(\mathbf{x}) \begin{bmatrix} \varepsilon_{11} \\ \varepsilon_{33} \\ 2\varepsilon_{13} \end{bmatrix} + \mathbf{H}(\mathbf{x}) \begin{bmatrix} E_1 \\ E_3 \end{bmatrix}, \quad (9) \end{aligned}$$

Recall that σ_{22} does not influence the governing equations, although it is not vanishing in general, since $\sigma_{22} = c_{21}\varepsilon_{11} + c_{23}\varepsilon_{33}$.

The following essential and natural boundary conditions are assumed for the mechanical field

$$u_i(\mathbf{x}) = \tilde{u}_i(\mathbf{x}), \text{ on } \Gamma_u,$$

$$t_i(\mathbf{x}) = \sigma_{ij}n_j = \tilde{t}_i(\mathbf{x}), \text{ on } \Gamma_t,$$

and for the electrical field

$$\begin{aligned} \psi(\mathbf{x}) &= \tilde{\psi}(\mathbf{x}), \text{ on } \Gamma_p, \\ n_i D_i(\mathbf{x}) &= \tilde{Q}(\mathbf{x}), \text{ on } \Gamma_q, \end{aligned}$$

where Γ_u is the part of the global boundary with prescribed displacements, and on Γ_t , Γ_p and Γ_q the traction vector, the electric potential and the surface charge density are prescribed, respectively.

On the upper and the lower crack-face Γ_c^+ and Γ_c^- , self-equilibrated generalized tractions are considered. Let's define the crack-opening displacement

$$\Delta u_3(\mathbf{x}, \tau) = u_3(\mathbf{x} \in \Gamma_c^+, \tau) - u_3(\mathbf{x} \in \Gamma_c^-, \tau).$$

Further, four different kinds of the electrical boundary conditions are considered on the crack-faces. The impermeable electrical crack-face condition

$$D_i(\mathbf{x} \in \Gamma_c^+, \tau) = D_i(\mathbf{x} \in \Gamma_c^-, \tau) = 0 \tag{10}$$

denotes in a physical sense that both crack-faces are free of electrical displacements. This would be correct for a medium inside the crack with electrical permittivity κ_c of zero. In contrast, the permeable electrical crack-face condition,

$$\begin{aligned} D_i(\mathbf{x} \in \Gamma_c^+, \tau) &= D_i(\mathbf{x} \in \Gamma_c^-, \tau) \\ \psi(\mathbf{x} \in \Gamma_c^+, \tau) - \psi(\mathbf{x} \in \Gamma_c^-, \tau) &= 0, \end{aligned} \tag{11}$$

implies identical potentials on both crack-faces and as a consequence the electrical crack-tip field vanishes. This condition would be correct either for a closed crack with an infinitely thin dielectric medium between the crack-faces or for an open crack with an infinite electrical permittivity. Since the impermeable as well as the permeable crack-face conditions are physically not consistent and the crack-tip fields have a major influence on the fracture parameters, Hao and Shen (1994) have introduced the more realistic semi-permeable crack-face condition

$$D_3(\mathbf{x} \in \Gamma_c^+, \tau) = D_3(\mathbf{x} \in \Gamma_c^-, \tau) = -\kappa_c \frac{\psi(\mathbf{x} \in \Gamma_c^+, \tau) - \psi(\mathbf{x} \in \Gamma_c^-, \tau)}{u_3(\mathbf{x} \in \Gamma_c^+, \tau) - u_3(\mathbf{x} \in \Gamma_c^-, \tau)}, \tag{12}$$

where both opposite crack-faces are considered as a set of corresponding parallel capacitors. In eq. (12), the electrical permittivity of the medium inside the crack is described by $\kappa_c = \kappa_r \cdot \kappa_0$, where $\kappa_0 = 0.854 \cdot 10^{-12} C/Vm$ is the permittivity of the vacuum and κ_r is a relative permittivity inside the crack. In contrast to the impermeable and permeable crack-face conditions a non-linear relation between

mechanical displacements, electrical displacements and electrical potential is now present.

Landis (2004) considered energetically consistent boundary conditions on the crack-faces, where an additional closing traction is added to the well-known semi-permeable crack-face boundary conditions

$$D_3(\mathbf{x} \in \Gamma_c^+, \tau) = D_3(\mathbf{x} \in \Gamma_c^-, \tau) = -\kappa_c \frac{\psi(\mathbf{x} \in \Gamma_c^+, \tau) - \psi(\mathbf{x} \in \Gamma_c^-, \tau)}{u_3(\mathbf{x} \in \Gamma_c^+, \tau) - u_3(\mathbf{x} \in \Gamma_c^-, \tau)},$$

$$t_3(\mathbf{x} \in \Gamma_c^+, \tau) = -t_3(\mathbf{x} \in \Gamma_c^-, \tau) = \frac{1}{2} \kappa_c \left[\frac{\psi(\mathbf{x} \in \Gamma_c^+, \tau) - \psi(\mathbf{x} \in \Gamma_c^-, \tau)}{u_3(\mathbf{x} \in \Gamma_c^+, \tau) - u_3(\mathbf{x} \in \Gamma_c^-, \tau)} \right]^2. \quad (13)$$

To solve the corresponding initial-boundary value problem, we apply the local integral equation method with meshless approximations. The MLPG method constructs a weak-form over the local fictitious subdomains such as Ω_s , which is a small region taken for each node inside the global domain [Atluri (2004)]. The local subdomains overlap each other, and cover the whole global domain Ω . The local subdomains could be of any geometrical shape and size. In the present paper, the local subdomains are taken to be of a circular shape for simplicity. The local weak-form of the governing equations (1) can be written as

$$\int_{\partial\Omega_s} \sigma_{ij}(\mathbf{x}, t) n_j(\mathbf{x}) u_{ik}^*(\mathbf{x}) d\Gamma - \int_{\Omega_s} \sigma_{ij}(\mathbf{x}, t) u_{ik,j}^*(\mathbf{x}) d\Omega$$

$$+ \int_{\Omega_s} [-\rho \ddot{u}_i(\mathbf{x}, t) + X_i(\mathbf{x}, t)] u_{ik}^*(\mathbf{x}) d\Omega = 0, \quad (14)$$

where $\partial\Omega_s$ is the boundary of the local subdomain which consists of three parts $\partial\Omega_s = L_s \cup \Gamma_{st} \cup \Gamma_{su}$ [Atluri, (2004)]. Here, L_s is the local boundary that is totally inside the global domain, Γ_{st} is the part of the local boundary which coincides with the global traction boundary, i.e., $\Gamma_{st} = \partial\Omega_s \cap \Gamma_t$, and similarly Γ_{su} is the part of the local boundary that coincides with the global displacement boundary, i.e., $\Gamma_{su} = \partial\Omega_s \cap \Gamma_u$.

By choosing a Heaviside step function as the test function $u_{ik}^*(\mathbf{x})$ in each subdomain

$$u_{ik}^*(\mathbf{x}) = \begin{cases} \delta_{ik} & \text{at } \mathbf{x} \in \Omega_s \\ 0 & \text{at } \mathbf{x} \notin \Omega_s \end{cases},$$

the local weak-form (14) is converted into the following local boundary-domain

integral equations

$$\int_{L_s+\Gamma_{su}} t_i(\mathbf{x}, \tau) d\Gamma - \int_{\Omega_s} \rho \ddot{u}_i(\mathbf{x}, \tau) d\Omega = - \int_{\Gamma_{st}} \tilde{t}_i(\mathbf{x}, \tau) d\Gamma - \int_{\Omega_s} X_i(\mathbf{x}, \tau) d\Omega. \quad (15)$$

Equation (15) is recognized as the overall force equilibrium conditions on the subdomain Ω_s . Note that the local integral equations (15) are valid for both the homogeneous and continuously nonhomogeneous solids. Nonhomogeneous material properties are included in eq. (15) through the elastic and piezoelectric coefficients involved in the traction components

$$t_i(\mathbf{x}, \tau) = [c_{ijkl}(\mathbf{x})u_{k,l}(\mathbf{x}, \tau) + e_{kij}(\mathbf{x})\psi_{,k}(\mathbf{x}, \tau)] n_j(\mathbf{x}).$$

Similarly, the local weak-form of the governing equation (2) can be written as

$$\int_{\Omega_s} [D_{j,j}(\mathbf{x}, \tau) - R(\mathbf{x}, \tau)] v^*(\mathbf{x}) d\Omega = 0, \quad (16)$$

where $v^*(\mathbf{x})$ is a test function.

Applying the Gauss divergence theorem to the local weak-form (16) and choosing the Heaviside step function as the test function $v^*(\mathbf{x})$, one can obtain

$$\int_{L_s+\Gamma_{sp}} Q(\mathbf{x}, \tau) d\Gamma = - \int_{\Gamma_{sq}} \tilde{Q}(\mathbf{x}, \tau) d\Gamma + \int_{\Omega_s} R(\mathbf{x}, \tau) d\Omega, \quad (17)$$

where

$$Q(\mathbf{x}, \tau) = D_j(\mathbf{x}, \tau) n_j(\mathbf{x}) = [e_{jkl}u_{k,l}(\mathbf{x}, \tau) - h_{jk}\psi_{,k}(\mathbf{x}, \tau)] n_j.$$

In the MLPG method the test and the trial functions are not necessarily from the same functional spaces. For internal nodes, the test function is chosen as a unit step function with its support on the local subdomain. The trial functions, on the other hand, are chosen to be the MLS approximations by using a number of nodes spreading over the domain of influence. According to the MLS [Belytschko et al., (1996)] method, the approximation of the displacement field can be given as

$$\mathbf{u}^h(\mathbf{x}) = \sum_{i=1}^m p_i(\mathbf{x}) a_i(\mathbf{x}) = \mathbf{p}^T(\mathbf{x}) \mathbf{a}(\mathbf{x}), \quad (18)$$

where $\mathbf{p}^T(\mathbf{x}) = \{p_1(\mathbf{x}), p_2(\mathbf{x}), \dots, p_m(\mathbf{x})\}$ is a vector of complete basis functions of order m and $\mathbf{a}(\mathbf{x}) = \{a_1(\mathbf{x}), a_2(\mathbf{x}), \dots, a_m(\mathbf{x})\}$ is a vector of unknown parameters which depend on \mathbf{x} . For example, in 2-D problems

$$\mathbf{p}^T(\mathbf{x}) = \{1, x_1, x_3\} \text{ for } m=3$$

and

$$\mathbf{p}^T(\mathbf{x}) = \{1, x_1, x_3, x_1^2, x_1 x_3, x_3^2\} \text{ for } m=6$$

are linear and quadratic basis functions, respectively. The basis functions are not necessary to be polynomials. It is convenient to introduce $r^{-1/2}$ - singularity for secondary fields at the crack-tip vicinity for modelling of fracture problems [Fleming et al., (1997)]. Then, the basis functions can be considered in the following form

$$\mathbf{p}^T(\mathbf{x}) = \{1, x_1, x_3, \sqrt{r} \cos(\theta/2), \sqrt{r} \sin(\theta/2), \sqrt{r} \sin(\theta/2) \sin \theta, \sqrt{r} \cos(\theta/2) \sin \theta\} \text{ for } m=7,$$

where r and θ are polar coordinates with the crack-tip as the origin. The upper given enriched basic functions represent all occurring terms in the asymptotic expansion of displacements at the crack-tip vicinity. Then, the density of the node distribution in such a case can be lower than in the case of pure polynomial basis functions in order to receive the same accuracy of results.

The approximated functions for the mechanical displacements and the electric potential can be written as [Atluri, (2004)]

$$\mathbf{u}^h(\mathbf{x}, \tau) = \mathbf{\Phi}^T(\mathbf{x}) \cdot \hat{\mathbf{u}} = \sum_{a=1}^n \phi^a(\mathbf{x}) \hat{\mathbf{u}}^a(\tau),$$

$$\psi^h(\mathbf{x}, \tau) = \sum_{a=1}^n \phi^a(\mathbf{x}) \hat{\psi}^a(\tau), \quad (19)$$

where the nodal values $\hat{\mathbf{u}}^a(\tau) = (\hat{u}_1^a(\tau), \hat{u}_3^a(\tau))^T$ and $\hat{\psi}^a(\tau)$ are fictitious parameters for the displacements and the electric potential, respectively, and $\phi^a(\mathbf{x})$ is the shape function associated with the node a . The number of nodes n used for the approximation is determined by the weight function $w^a(\mathbf{x})$. A 4th order spline-type weight function is applied in the present work

$$w^a(\mathbf{x}) = \begin{cases} 1 - 6 \left(\frac{d^a}{r^a}\right)^2 + 8 \left(\frac{d^a}{r^a}\right)^3 - 3 \left(\frac{d^a}{r^a}\right)^4, & 0 \leq d^a \leq r^a \\ 0, & d^a \geq r^a \end{cases}, \quad (20)$$

where $d^a = \|\mathbf{x} - \mathbf{x}^a\|$ and r^a is the size of the support domain. It is seen that the C^1 -continuity is ensured over the entire domain, and therefore the continuity conditions of the tractions and the electric charge are satisfied. In the MLS approximation the rates of the convergence of the solution may depend upon the nodal distance as well as the size of the support domain [Wen and Aliabadi (2007, 2008), Wen et al., (2008)]. It should be noted that a smaller size of the subdomains may

induce larger oscillations in the nodal shape functions [Atluri (2004)]. A necessary condition for a regular MLS approximation is that at least m weight functions are non-zero (i.e. $n \geq m$) for each sample point $\mathbf{x} \in \Omega$. This condition determines the size of the support domain.

Then, the traction vector $t_i(\mathbf{x}, \tau)$ at a boundary point $\mathbf{x} \in \partial\Omega_s$ is approximated in terms of the same nodal values $\hat{\mathbf{u}}^a(\tau)$ as

$$\mathbf{t}^h(\mathbf{x}, \tau) = \mathbf{N}(\mathbf{x})\mathbf{C}(\mathbf{x}) \sum_{a=1}^n \mathbf{B}^a(\mathbf{x})\hat{\mathbf{u}}^a(\tau) + \mathbf{N}(\mathbf{x})\mathbf{L}(\mathbf{x}) \sum_{a=1}^n \mathbf{P}^a(\mathbf{x})\hat{\psi}^a(\tau), \quad (21)$$

where the matrices $\mathbf{C}(\mathbf{x})$, $\mathbf{L}(\mathbf{x})$ are defined in eq. (8) and the matrix $\mathbf{N}(\mathbf{x})$ is related to the normal vector $\mathbf{n}(\mathbf{x})$ on $\partial\Omega_s$ by

$$\mathbf{N}(\mathbf{x}) = \begin{bmatrix} n_1 & 0 & n_3 \\ 0 & n_3 & n_1 \end{bmatrix},$$

and finally, the matrices \mathbf{B}^a and \mathbf{P}^a are represented by the gradients of the shape functions as

$$\mathbf{B}^a(\mathbf{x}) = \begin{bmatrix} \phi_{,1}^a & 0 \\ 0 & \phi_{,3}^a \\ \phi_{,3}^a & \phi_{,1}^a \end{bmatrix}, \quad \mathbf{P}^a(\mathbf{x}) = \begin{bmatrix} \phi_{,1}^a \\ \phi_{,3}^a \end{bmatrix}.$$

Similarly the normal component of the electric displacement vector $Q(\mathbf{x}, \tau)$ can be approximated by

$$Q^h(\mathbf{x}, \tau) = \mathbf{N}_1(\mathbf{x})\mathbf{G}(\mathbf{x}) \sum_{a=1}^n \mathbf{B}^a(\mathbf{x})\hat{\mathbf{u}}^a(\tau) - \mathbf{N}_1(\mathbf{x})\mathbf{H}(\mathbf{x}) \sum_{a=1}^n \mathbf{P}^a(\mathbf{x})\hat{\psi}^a(\tau), \quad (22)$$

where the matrices $\mathbf{G}(\mathbf{x})$, $\mathbf{H}(\mathbf{x})$ are defined in eq. (9) and

$$\mathbf{N}_1(\mathbf{x}) = \begin{bmatrix} n_1 & n_3 \end{bmatrix}.$$

Satisfying the essential boundary conditions and making use of the approximation formulae (19), one obtains the discretized form of these boundary conditions as

$$\begin{aligned} \sum_{a=1}^n \phi^a(\boldsymbol{\zeta})\hat{\mathbf{u}}^a(\tau) &= \tilde{\mathbf{u}}(\boldsymbol{\zeta}, \tau) \text{ for } \boldsymbol{\zeta} \in \Gamma_u, \\ \sum_{a=1}^n \phi^a(\boldsymbol{\zeta})\hat{\psi}^a(\tau) &= \tilde{\psi}(\boldsymbol{\zeta}, \tau) \text{ for } \boldsymbol{\zeta} \in \Gamma_p. \end{aligned} \quad (23)$$

Furthermore, in view of the MLS-approximations (21) and (22) for the unknown quantities in the local boundary-domain integral equations (15) and (17), we obtain their discretized forms as

$$\sum_{a=1}^n \left[\left(\int_{L_s + \Gamma_{st}} \mathbf{N}(\mathbf{x}) \mathbf{C}(\mathbf{x}) \mathbf{B}^a(\mathbf{x}) d\Gamma \right) \hat{\mathbf{u}}^a(\tau) - \left(\int_{\Omega_s} \rho(\mathbf{x}) \varphi^a d\Omega \right) \ddot{\mathbf{u}}^a(\tau) \right] + \sum_{a=1}^n \left(\int_{L_s + \Gamma_{st}} \mathbf{N}(\mathbf{x}) \mathbf{L}(\mathbf{x}) \mathbf{P}^a(\mathbf{x}) d\Gamma \right) \hat{\psi}^a(\tau) = - \int_{\Gamma_{st}} \tilde{\mathbf{t}}(\mathbf{x}, \tau) d\Gamma - \int_{\Omega_s} \mathbf{X}(\mathbf{x}, \tau) d\Omega, \quad (24)$$

$$\sum_{a=1}^n \left(\int_{L_s + \Gamma_{sq}} \mathbf{N}_1(\mathbf{x}) \mathbf{G}(\mathbf{x}) \mathbf{B}^a(\mathbf{x}) d\Gamma \right) \hat{\mathbf{u}}^a(\tau) - \sum_{a=1}^n \left(\int_{L_s + \Gamma_{sq}} \mathbf{N}_1(\mathbf{x}) \mathbf{H}(\mathbf{x}) \mathbf{P}^a(\mathbf{x}) d\Gamma \right) \hat{\psi}^a(\tau) = - \int_{\Gamma_{sq}} \tilde{\mathcal{Q}}(\mathbf{x}, \tau) d\Gamma + \int_{\Omega_s} R(\mathbf{x}, \tau) d\Omega, \quad (25)$$

which are considered on the sub-domains adjacent to the interior nodes as well as to the boundary nodes on Γ_{st} and Γ_{sq} .

Collecting the discretized local boundary-domain integral equations together with the discretized boundary conditions for the displacements and the electrical potential results in a complete system of ordinary differential equations and it can be rearranged in such a way that all known quantities are on the r.h.s. Thus, in matrix form the system becomes

$$\mathbf{A}\ddot{\mathbf{x}} + \mathbf{C}\mathbf{x} = \mathbf{Y}. \quad (26)$$

There are many time integration procedures for the solution of this system of ordinary differential equations. In the present work, the Houbolt method is applied. In the Houbolt finite- difference scheme [Houbolt (1950)], the “acceleration” ($\ddot{\mathbf{u}} = \ddot{\mathbf{x}}$) is expressed as

$$\ddot{\mathbf{x}}_{\tau+\Delta\tau} = \frac{2\mathbf{x}_{\tau+\Delta\tau} - 5\mathbf{x}_{\tau} + 4\mathbf{x}_{\tau-\Delta\tau} - \mathbf{x}_{\tau-2\Delta\tau}}{\Delta\tau^2}, \quad (27)$$

where $\Delta\tau$ is the time-step.

Substituting eq. (27) into eq. (26), we get the following system of algebraic equations for the unknowns $\mathbf{x}_{\tau+\Delta\tau}$

$$\left[\frac{2}{\Delta\tau^2} \mathbf{A} + \mathbf{C} \right] \mathbf{x}_{\tau+\Delta\tau} = \frac{5\mathbf{A}}{\Delta\tau^2} \mathbf{x}_{\tau} + \mathbf{A} \frac{1}{\Delta\tau^2} \{ -4\mathbf{x}_{\tau-\Delta\tau} + \mathbf{x}_{\tau-2\Delta\tau} \} + \mathbf{Y}. \quad (28)$$

The value of the time-step has to be appropriately selected with respect to material parameters (wave velocities) and time dependence of the boundary conditions.

3 Numerical procedure for non-linear crack-face boundary conditions

There are more possibilities to solve the boundary value problem with non-linear crack-face boundary conditions. The simplest way is to use an iterative algorithm at each time-step for electrical displacement in n-th iteration [Enderlein et al. 2005]

$$D_3^{(n)}(\mathbf{x}, \tau) = -\kappa_c \frac{\Delta\psi^{(n-1)}(\mathbf{x}, \tau)}{\Delta u_3^{(n-1)}(\mathbf{x}, \tau)}. \tag{29}$$

In the first iteration step impermeable boundary conditions are considered on the crack-faces. This approach requires a lot of iteration steps if the crack opening displacement is small at a low load level. More efficient is the Newton-Raphson scheme. If the residuum of the electrical displacement expression is denoted as

$$R(D_3) = D_3(\mathbf{x}, t) + \kappa_c \frac{\Delta\psi(\mathbf{x}, \tau, D_3)}{\Delta u_3(\mathbf{x}, \tau, D_3)}$$

the electrical displacement value at (n+1)-th iteration step is given by the Newton-Raphson scheme as

$$D_3^{(n+1)} = D_3^{(n)} - \left[\frac{\partial R(D_3^{(n)})}{\partial D_3^{(n)}} \right]^{-1} R(D_3^{(n)}).$$

Replacing the differentiation by the ratio of differences, one obtains

$$D_3^{(n+1)} = D_3^{(n)} - \left[1 + \kappa_c \frac{\Delta u_3^{(n-1)} \Delta\psi^{(n)} - \Delta u_3^{(n)} \Delta\psi^{(n-1)}}{(\Delta u_3^{(n)})^2 (D_3^{(n)} - D_3^{(n-1)})} \right]^{-1} \left(D_3^{(n)} + \kappa_c \frac{\Delta\psi^{(n)}}{\Delta u_3^{(n)}} \right). \tag{30}$$

Denda (2008) suggested a numerical procedure based on the knowledge that the semi-permeable solution is somewhere in between the impermeable and permeable crack solutions. The iteration procedure has the following steps applied in each time-step (not distinguished in the notations):

1. compute the electrical potential jump $\Delta\psi^{(0)}(\mathbf{x})$ on the crack for given problem with impermeable boundary conditions

2. in the k-th iteration step, slightly reduce the value of the electrical potential jump by a control parameter p^k , $\Delta\psi(\mathbf{x}, p^k) = p^k \Delta\psi(\mathbf{x}, p^{k-1})$, where $p^k \in (0, 1)$ and $\Delta\psi(\mathbf{x}, p^0) = \Delta\psi^{(0)}(\mathbf{x})$
3. solving the problem with prescribed $\Delta\psi(\mathbf{x}, p^k)$, compute the electrical displacement $D_3(\mathbf{x}, p^k)$ and $\Delta u_3(\mathbf{x}, p^k)$
4. calculate the crack permittivity $\kappa_c(\mathbf{x}, p^k) = -D_3(\mathbf{x}, p^k) \frac{\Delta u_3(\mathbf{x}, p^k)}{\Delta\psi(\mathbf{x}, p^k)}$
5. calculate the average value of the crack permittivity $\bar{\kappa}_c(p^k)$ from all nodal values computed in the previous step
6. repeat the steps b) to f) for progressively reduced value of the control parameter p^{k+1} to plot $\bar{\kappa}_c(p^k)$ - p^k curve
7. the intersection of the $\bar{\kappa}_c(p^k)$ - p^k curve and the horizontal line with prescribed crack permittivity κ_c gives the control parameter value p^c for which the semi-permeable solution can be obtained easily.

The Denda's approach can be easily extended to the model with energetically consistent boundary conditions on the crack-faces. In numerical examples, we have used the Newton-Raphson scheme.

4 Computation of the dynamic intensity factors

Jin and Noda (1994), and Eischen (1987) showed that the nature of the stress singularity in continuously nonhomogeneous solids has precisely the same well-known form applicable to homogeneous elastic materials. Later Sladek et al. (2007b) extended that validity to piezoelectric materials too. In the crack-tip vicinity, the displacements as well as the electric potential show the classical \sqrt{r} asymptotic behaviour. Hence, correspondingly, the stresses and the electrical displacements exhibit a $1/\sqrt{r}$ -behaviour, where r is the radial polar coordinate with the origin at the crack-tip. For cracks in homogeneous piezoelectric media the asymptotic behaviour of the field quantities has been given by Sosa (1991) and Pak (1992). If polar coordinates (r, θ) with the origin at the crack-tip are used, the electromechanical fields can be written as

$$\sigma_{ij}(r, \theta) = \frac{1}{\sqrt{2\pi r}} \sum_{N=1}^4 K_N f_{ij}^N(\theta), \quad D_i(r, \theta) = \frac{1}{\sqrt{2\pi r}} \sum_{N=1}^4 K_N g_i^N(\theta), \quad (31)$$

$$u_i(r, \theta) = \sqrt{\frac{2r}{\pi}} \sum_{N=1}^4 K_N d_i^N(\theta), \quad \psi(r, \theta) = \sqrt{\frac{2r}{\pi}} \sum_{N=1}^4 K_N v^N(\theta), \quad (32)$$

where K_I , K_{II} and K_{III} denote the well-known mechanical stress intensity factors (SIF) and K_{IV} is the electrical displacement intensity factor (EDIF). The angular functions $f_{ij}^N(\theta)$, $g_i^N(\theta)$, $d_i^N(\theta)$ and $v^N(\theta)$ are dependent on the material properties only and given by

$$f_{i1}^N = - \sum_{\alpha=1}^4 Re \left\{ \frac{M_{i\alpha} N_{\alpha N} P_{\alpha}}{\sqrt{\cos \theta + p_{\alpha} \sin \theta}} \right\}, \quad f_{i2}^N = \sum_{\alpha=1}^4 Re \left\{ \frac{M_{i\alpha} N_{\alpha N}}{\sqrt{\cos \theta + p_{\alpha} \sin \theta}} \right\},$$

$$g_1^N = - \sum_{\alpha=1}^4 Re \left\{ \frac{M_{4\alpha} N_{\alpha N} P_{\alpha}}{\sqrt{\cos \theta + p_{\alpha} \sin \theta}} \right\}, \quad g_2^N = \sum_{\alpha=1}^4 Re \left\{ \frac{M_{4\alpha} N_{\alpha N}}{\sqrt{\cos \theta + p_{\alpha} \sin \theta}} \right\},$$

$$d_i^N = \sum_{\alpha=1}^4 Re \left\{ A_{i\alpha} N_{\alpha N} \sqrt{\cos \theta + p_{\alpha} \sin \theta} \right\},$$

$$v^N = \sum_{\alpha=1}^4 Re \left\{ A_{4\alpha} N_{\alpha N} \sqrt{\cos \theta + p_{\alpha} \sin \theta} \right\},$$

where p_{α} are eigenvalues of the characteristic equations for an anisotropic body and the matrices $A_{i\alpha}$, $M_{i\alpha}$ and $N_{\alpha N}$ are defined in the work [Park and Sun (1995)]. From equations (32) one can derive the expressions for the generalized intensity factors

$$\begin{pmatrix} K_{II} \\ K_I \\ K_{IV} \end{pmatrix} = \lim_{r \rightarrow 0} \sqrt{\frac{2\pi}{r}} \mathbf{H} \begin{pmatrix} u_1 \\ u_3 \\ \psi \end{pmatrix}, \tag{33}$$

where the matrix \mathbf{H} is determined by the material properties (Suo et al. 1992, Wünsche et al. 2010) and/or

$$K_I = \lim_{r \rightarrow 0} \sqrt{2\pi r} \sigma_{33}(r, 0),$$

$$K_{II} = \lim_{r \rightarrow 0} \sqrt{2\pi r} \sigma_{13}(r, 0),$$

$$K_{IV} = \lim_{r \rightarrow 0} \sqrt{2\pi r} D_3(r, 0).$$

5 Numerical examples

5.1 A central crack in a finite homogeneous strip

In the first example a straight central crack in a homogeneous finite strip under uniform mechanical and electrical loads is analyzed (Fig. 1). The strip is subjected to a stationary or impact mechanical load with Heaviside time variation and the intensity $\sigma_0 = 10^8 Pa$ and an electrical load with $D_0 = 10^{-2} Cm^{-2}$ on the top side of the strip. Homogeneous material properties are selected to test the present computational method. The material coefficients of the strip correspond to the PZT-4 material and they are given by

$$c_{11} = 13.9 \cdot 10^{10} Nm^{-2}, \quad c_{13} = 7.43 \cdot 10^{10} Nm^{-2},$$

$$c_{33} = 11.5 \cdot 10^{10} Nm^{-2}, \quad c_{44} = 2.56 \cdot 10^{10} Nm^{-2},$$

$$e_{15} = 12.7 Cm^{-2}, \quad e_{31} = -5.2 Cm^{-2}, \quad e_{33} = 15.1 Cm^{-2},$$

$$h_{11} = 6.46 \cdot 10^{-9} C(Vm)^{-1}, \quad h_{33} = 5.62 \cdot 10^{-9} C(Vm)^{-1}, \quad \rho = 7500 kg / m^3.$$

The crack-length $2a = 1.0m$, strip width ratio $a/w = 0.4$, and height of the strip $h = 1.2w$ are considered. Due to the symmetry of the problem with respect to the crack-line, only a quarter of the specimen is numerically analyzed. The mechanical displacement and the electrical potential fields in the quarter of the specimen are approximated by using 930 (31x30) nodes equidistantly distributed. The local subdomains are considered to be circular with a radius $r_{loc} = 0.033m$.

Numerical results for the crack displacement u_3 along x_1 -direction for impermeable, permeable and semi-permeable crack conditions are given in Fig. 2. A pure mechanical static load $\sigma_0 = 10^8 Pa$ on the top side of the specimen is considered. One can observe a good agreement between the BIE and present MLPG results for all three electrical crack-face boundary conditions. The largest crack opening displacement is occurred at permeable electrical crack-face conditions.

From the comparison of the crack opening displacements for semi-permeable and energetically consistent crack boundary conditions (exact) on Fig. 3 it is seen a vanishing influence of closing tractions in energetically consistent crack boundary conditions on this value.

The variations of the electrical potential along the crack for impermeable and semi-permeable crack boundary conditions are given in Fig. 4. The BIE and MLPG results are in a good agreement. The electrical potential along the crack for the permeable crack-face condition is vanishing. The closing tractions in energetically consistent crack boundary conditions have almost vanishing influence on the

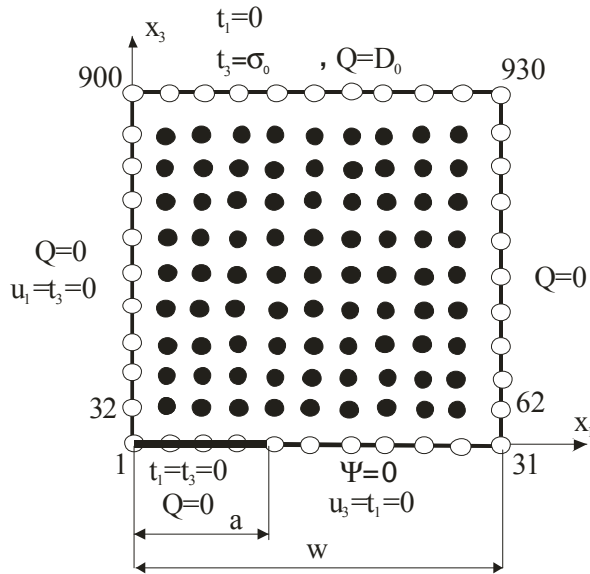


Figure 1: Central crack in a finite homogeneous strip

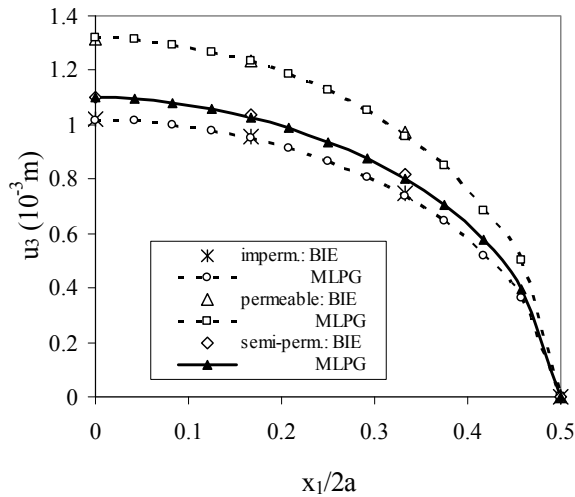


Figure 2: Variations of the crack displacement with the normalized coordinate $x_1/2a$ for a pure mechanical loading $\sigma_0 = 10^8 Pa$

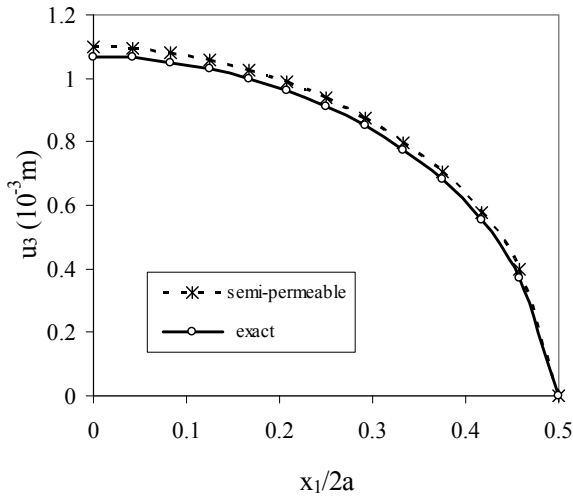


Figure 3: Comparison of the crack displacement for semi-permeable and energetically consistent crack b.c. under a pure mechanical loading $\sigma_0 = 10^8 Pa$

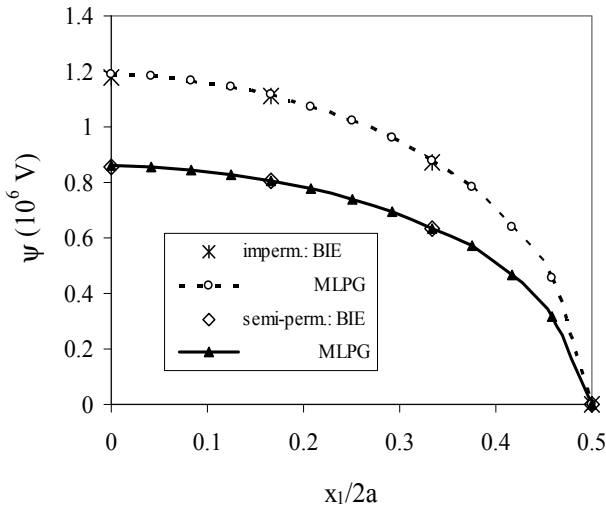


Figure 4: Variations of the electrical potential with the normalized coordinate $x_1/2a$ for a pure mechanical load

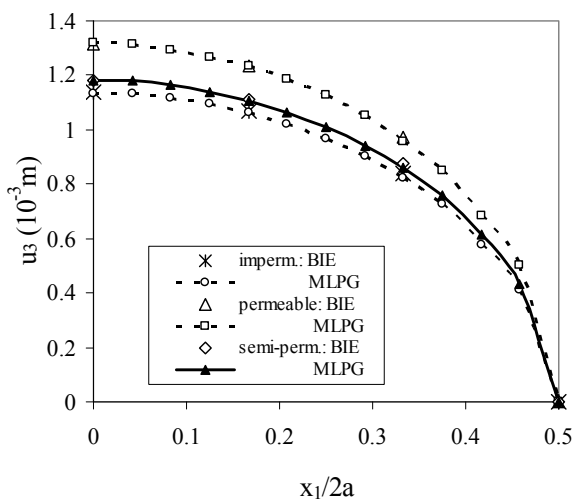


Figure 5: Variations of the crack displacement with the normalized coordinate $x_1/2a$ for a combination of mechanical and electrical loads

electrical potential, therefore the results are very close to the potential for the semi-permeable crack-face boundary condition.

In the next example we consider a combination of mechanical load $\sigma_0 = 10^8 Pa$ and electrical load with $D_0 = 10^{-2} Cm^{-2}$ on the top side of the strip. The crack opening displacement for impermeable, permeable and semi-permeable crack-face conditions are given in Fig. 5. One can observe again a good agreement of the present MLPG and the BIE results. At considered loading levels the semi-permeable results are closer to impermeable crack opening displacement than in the previous pure mechanical load. At the combined load the displacement values are larger. Smaller crack opening displacement is occurring at a lower load level. Therefore, we have considered a pure mechanical load with $\sigma_0 = 10^7 Pa$. Smaller displacement values at the same crack permittivity and semi-permeable crack-face boundary conditions are approaching permeable quantities in Fig. 6. It shows on a nonlinear character of semi-permeable boundary conditions.

The variations of the electrical potential along the crack for impermeable and semi-permeable crack-face boundary conditions at the combined load are given in Fig. 7. The BIE and MLPG results are in a good agreement.

Sladek et al. (2007a) observed that the electrical potential on the crack ψ caused by a remote stress loading σ_0 is identical to the crack opening displacement u_3 caused

by a remote electric displacement loading D_0 as a consequence of the extended Betti's reciprocal theorem. For a pure positive electrical displacement loading $K_I = 0$, therefore we obtain from eq. (32) a positive crack opening displacement u_3 and a negative electrical potential ψ . It is interesting to note that for a pure mechanical load, a finite value of the potential ψ on the crack does not result in a finite value of the EDIF K_{IV} . It means that the crack opening displacement u_3 and the potential jump ψ are coupled, but the SIF and the EDIF in this case are uncoupled. For a pure mechanical load we have obtained $K_I^{stat} = 1.428\text{Pa} \cdot \text{m}^{1/2}$ at $\sigma_0 = 10^8\text{Pa}$.

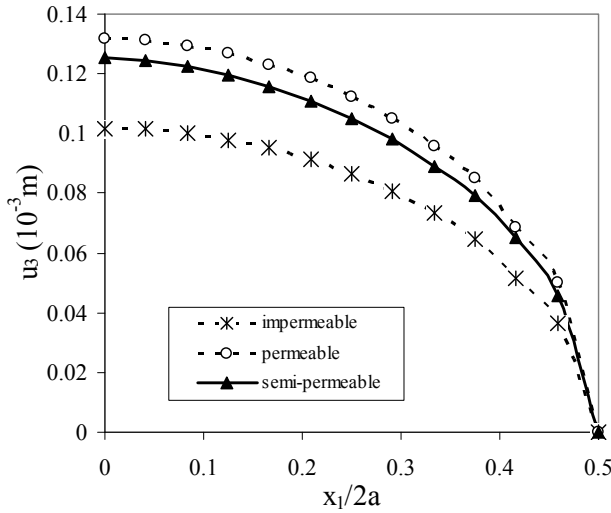


Figure 6: Variations of the crack opening displacement with the normalized coordinate $x_1/2a$ for pure mechanical loading $\sigma_0 = 10^7\text{Pa}$

In the next example we analyze the same cracked strip under a pure mechanical load with Heaviside time variation $\sigma_0 H(t - 0)$. The impermeable conditions are considered on the crack-faces. The normalized stress intensity factor K_I/K_I^{stat} and electrical displacement factor $\Lambda K_{IV}/K_I^{stat}$ are compared with the BIE results in Figs. 8 and 9, where $\Lambda = e_{22}/h_{22}$. The BIE results are obtained by a combination of the collocation method and the Galerkin-method with 102 linear elements for the full specimen and 100 time-steps. The temporal discretization is performed by the collocation method, while the spatial discretization is carried out by the Galerkin-method.

One can observe very good agreement of BIE and MLPG results for the SIF in Fig. 8. A slight difference is observed for the EDIF, since the value of EDIF is small for

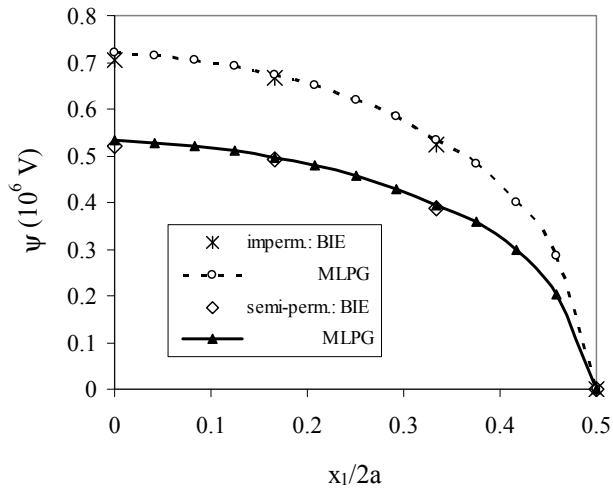


Figure 7: Variations of the electrical potential with the normalized coordinate $x_1/2a$ for a combination of mechanical and electrical loads

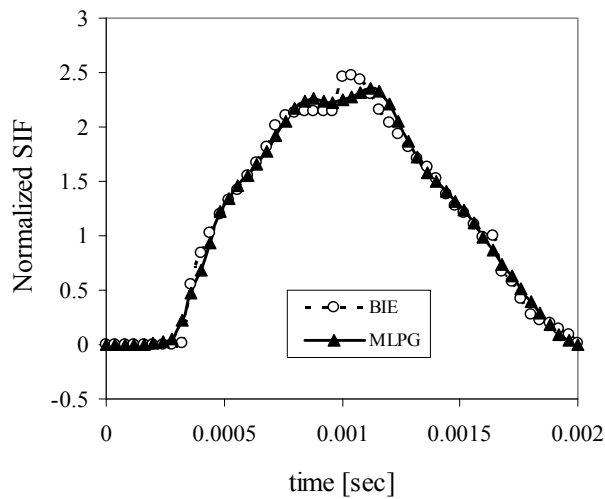


Figure 8: Temporal variation of the normalized SIF for a central crack in a strip under a pure mechanical impact load with $\sigma_0 = 10^8 Pa$

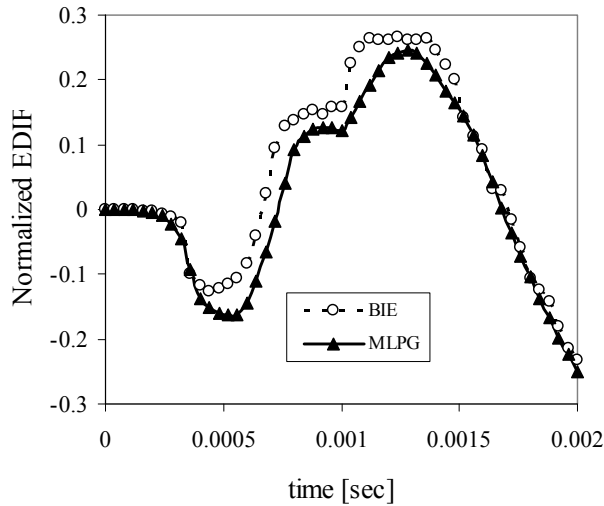


Figure 9: Temporal variation of the normalized EDIF for a central crack in a strip under a pure mechanical impact load with $\sigma_0 = 10^8 Pa$

impermeable conditions. The peak value of the dynamic SIF is more than doubled with respect to the static one. The electrical displacement intensity factor for a pure static mechanical load is vanishing as we stated above. Contrary to the static case the EDIF is not vanishing in the dynamic case with a finite velocity of wave propagation for a pure mechanical load. From the Maxwell's equations, it is known that the velocity of electromagnetic waves is equal to the speed of light, which is much larger than the velocity of elastic waves. The response of the electric field is immediate, while that of the elastic ones is taken as finite because of the finite velocity of elastic waves. On the other hand, in a static case, the response of both the mechanical (strain, stress) and electrical fields is immediate. Thus, the SIF is vanishing in such a case since the stress σ_{33} is zero ahead of the crack-tip on the crack-line because of the immediate electromechanical interaction. In the dynamic case the stress field is coupled not only to the immediate electric field, but also to inertia forces [Enderlein et al. (2005)]. One can observe from Fig. 10 that the three various electrical crack-face conditions have almost vanishing influence on the SIF in a cracked strip under a pure impact mechanical load.

However, the electrical crack-face conditions have strong influence on the EDIF for a cracked strip under a pure mechanical impact load. The largest EDIF corresponds to permeable crack-face conditions. The variation of the normalized dynamic EDIF

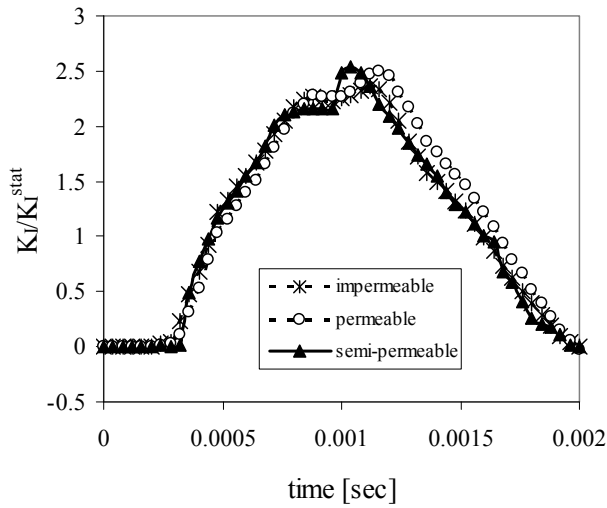


Figure 10: Influence of electrical crack-face conditions on the SIF for a cracked strip under a pure mechanical impact load $\sigma_0 H(t-0)$

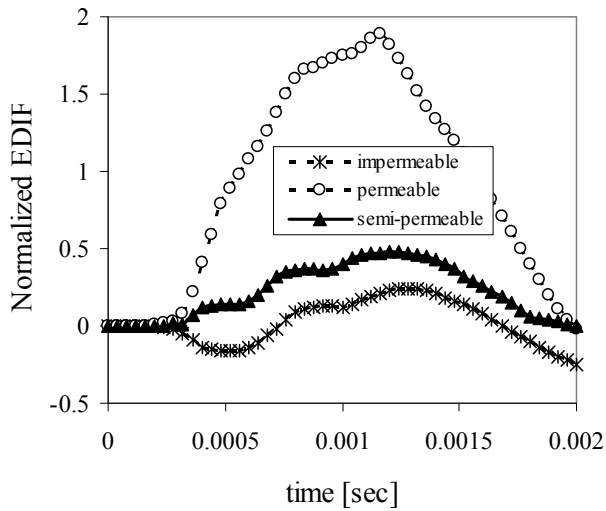


Figure 11: Influence of electrical crack-face conditions on the EDIF for a cracked strip under a pure mechanical impact load $\sigma_0 H(t-0)$

for permeable electrical crack-face boundary conditions is similar to the variation of the normalized dynamic SIF. The smallest EDIF corresponds to the impermeable crack-face conditions.

5.2 An edge crack in a finite FGPM strip

An edge crack in a finite strip is analyzed in the second example. The sample geometry is given in Fig. 12 with the following values: $a = 0.5$, $a/w = 0.4$ and $h/w = 1.2$. Due to the symmetry with respect to x_1 only a half of the specimen is modeled. We have used 930 nodes equidistantly distributed for the MLS approximation of the physical fields. On the top of the strip a uniform impact tension $\sigma_0 = 10^8 Pa$ and electrical displacement $D_0 = 10^{-2} Cm^{-2}$ are applied, respectively. Functionally graded material properties in x_1 -direction are considered. An exponential variation for the elastic, piezoelectric and dielectric tensors is used

$$\begin{aligned} c_{ijkl}(\mathbf{x}) &= c_{ijkl0} \exp(\gamma x_1), \\ e_{ijk}(\mathbf{x}) &= e_{ijk0} \exp(\gamma x_1), \\ h_{ij}(\mathbf{x}) &= h_{ij0} \exp(\gamma x_1), \end{aligned} \quad (34)$$

where c_{ijkl0} , e_{ijk0} and h_{ij0} correspond to the material parameters used in the previous example.

First, we present numerical results for a homogeneous cracked strip. The variations of the crack opening displacement along the crack-line for four various crack conditions are presented in Fig. 13. Similarly to the previous central crack the largest crack opening displacement is observed at permeable crack-face condition. The results for semi-permeable and energetically consistent crack conditions are very similar and they are approaching to impermeable results. The variations of the electrical potential for three various electrical crack-face conditions are presented in Fig. 14. The results for semi-permeable and energetically consistent crack-face conditions are again very similar. Their magnitudes are smaller than the ones for permeable crack-face conditions.

In the next example we analyze the same cracked strip under a combination of mechanical load with Heaviside time variation $\sigma_0 H(t - 0)$, where $\sigma_0 = 10^8 Pa$, and electrical impact load with $D_0 = 10^{-2} Cm^{-2}$ on the top side of the strip. Both impermeable and permeable conditions are considered on the crack-faces. The normalized stress intensity factor K_I/K_I^{stat} for both crack-face boundary conditions are presented in Figs. 15 and 16. The static stress intensity factor for the considered load and geometry is equal to $K_I^{stat} = 2.642 Pa m^{1/2}$. One can observe a quite good agreement of the FEM using ANSYS and the MLPG results. In the MLPG analysis we have used the time-step $\Delta\tau = 0.2 \cdot 10^{-4} s$.

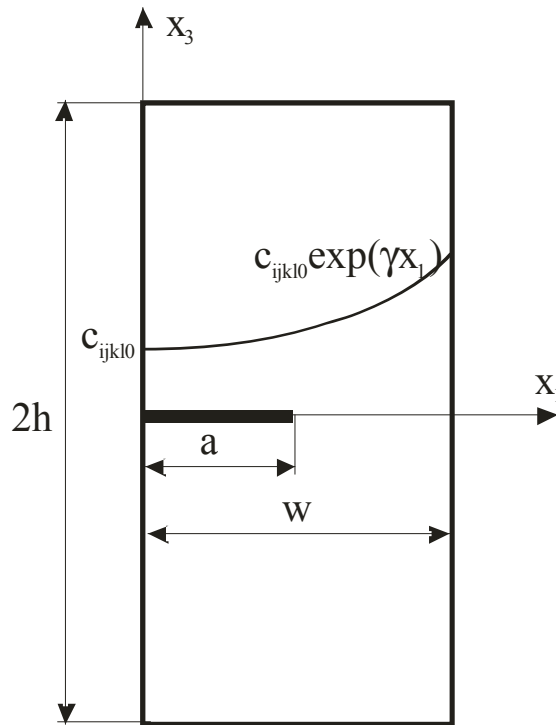


Figure 12: An edge crack in a finite strip with graded material properties in x_1 -direction

One can observe from Fig. 17 that the three various electrical crack-face conditions have almost vanishing influence on the SIF in a cracked strip under a combined electro-mechanical impact load.

The normalized electrical displacement intensity factor $\Lambda K_{IV} / K_I^{stat}$ is presented in Fig. 18. The electrical crack-face conditions have an influence on the EDIF for a cracked strip under a combined electro-mechanical impact load. The largest EDIF corresponds to the permeable crack-face condition.

Now, we consider the same exponential gradient for all material coefficients with the value $\gamma = 2m^{-1}$ in the numerical calculations. Then, all material parameters at the crack-tip are $e^1 = 2.718$ times larger than in the homogeneous material. Three various electrical boundary conditions on the crack-faces are considered. The numerical results for normalized SIF and EDIF are given in Figs. 19 and 20.

One can observe from Figs. 19 and 20 that the three various electrical crack-face conditions have almost vanishing influence on the SIF in the FGPM cracked strip.

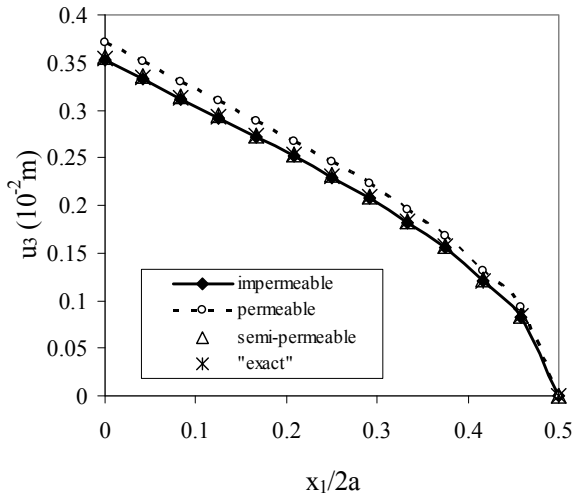


Figure 13: Variations of the crack displacement with the normalized coordinate $x_1/2a$ for a combination of mechanical and electrical loads in a homogeneous strip

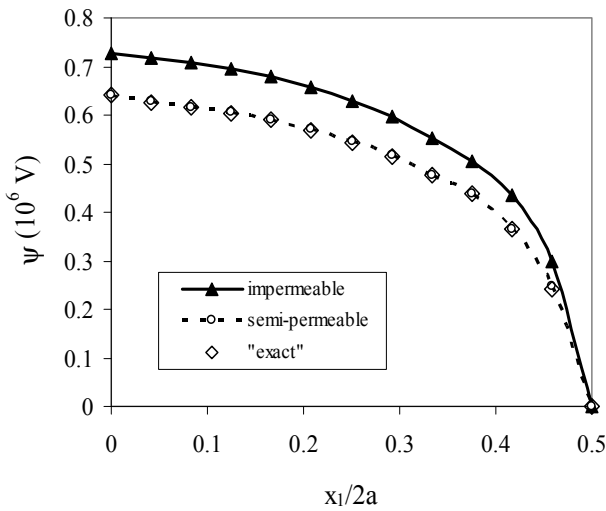


Figure 14: Variations of the electrical potential with the normalized coordinate $x_1/2a$ for a combination of mechanical and electrical loads in a homogeneous strip

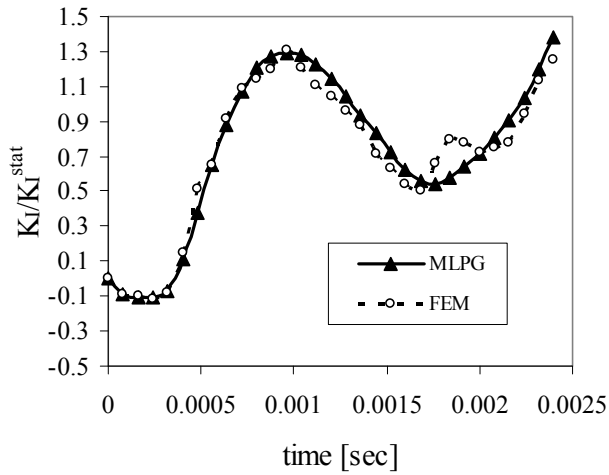


Figure 15: Temporal variation of the normalized SIF for an edge crack in a strip under a combined impact load with impermeable crack-face b.c.

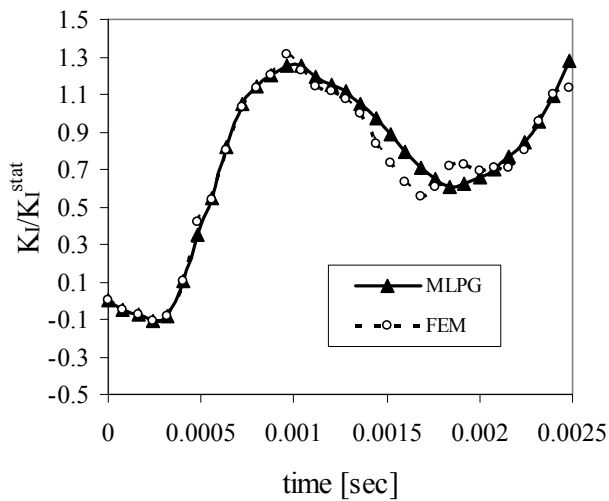


Figure 16: Temporal variation of the normalized SIF for an edge crack in a strip under a combined impact load with permeable crack-face b.c.

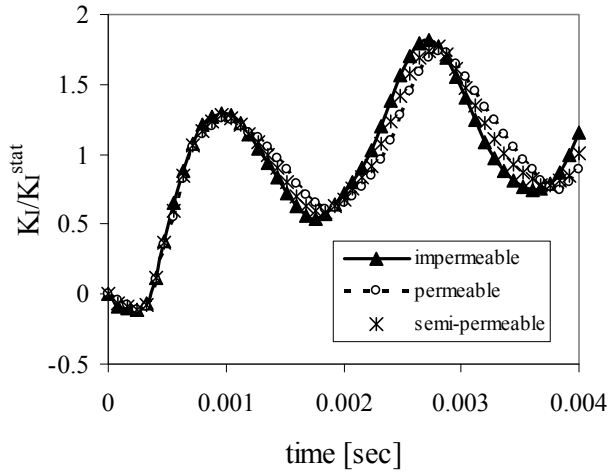


Figure 17: Influence of electrical crack-face conditions on the SIF for a cracked strip under a combined electro-mechanical impact load

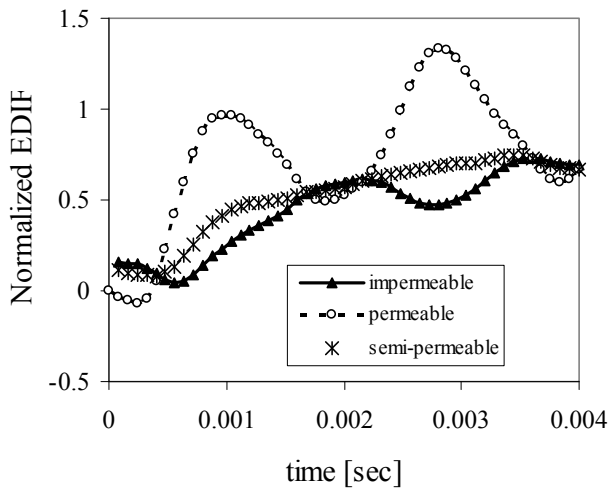


Figure 18: Influence of electrical crack-face conditions on the EDIF for a cracked strip under a combined electro-mechanical impact load

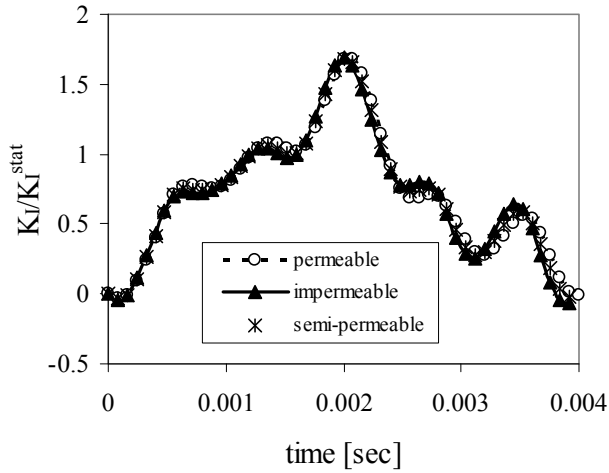


Figure 19: Influence of electrical crack-face conditions on the SIF for the FGPM cracked strip under a combined electro-mechanical impact load

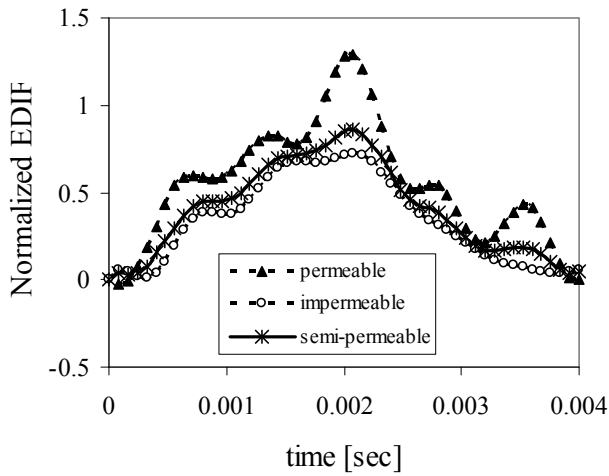


Figure 20: Influence of electrical crack-face conditions on the EDIF for the FGPM cracked strip under a combined electro-mechanical impact load

However, the electrical crack-face conditions have strong influence on the EDIF. Similar phenomenon has been observed in the previous example with a central

crack in a homogeneous material. The largest EDIF corresponds to permeable crack-face condition. The variation of the normalized dynamic EDIF for permeable electrical crack-face boundary condition is similar to the variation of the normalized dynamic SIF. The smallest EDIF corresponds to the impermeable crack-face condition.

The influence of the material gradation on the stress intensity factor and the electrical displacement intensity factor is analyzed too. The temporal variations of the SIF and the EDIF in the cracked FGPM strip are presented in Figs. 21 and 22, respectively. Numerical results are given for semi-permeable boundary conditions on the crack-faces.

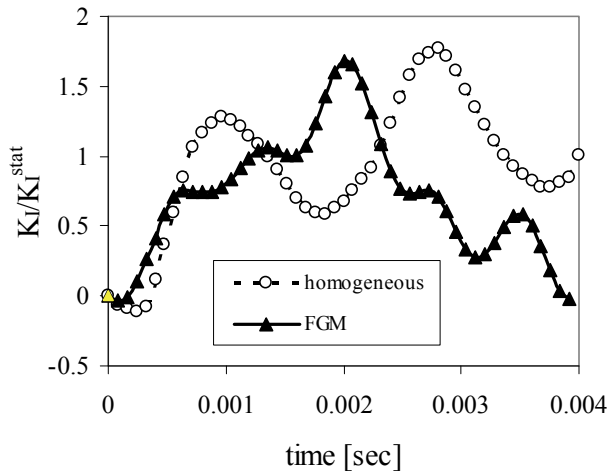


Figure 21: Temporal variations of the normalized SIF for an edge crack in a homogeneous and FGPM strip with semi-permeable crack-face condition

For a material gradation of the mechanical properties in the x_1 -direction and a uniform mass density, the wave propagation is growing with x_1 . Therefore, the peak value of the SIF is reached in a shorter time instant in the FGPM strip than in a homogeneous one. The maximum values of the SIF are almost the same in both homogeneous and FGPM cracked strip. Similar conclusion can be drawn for the EDIF.

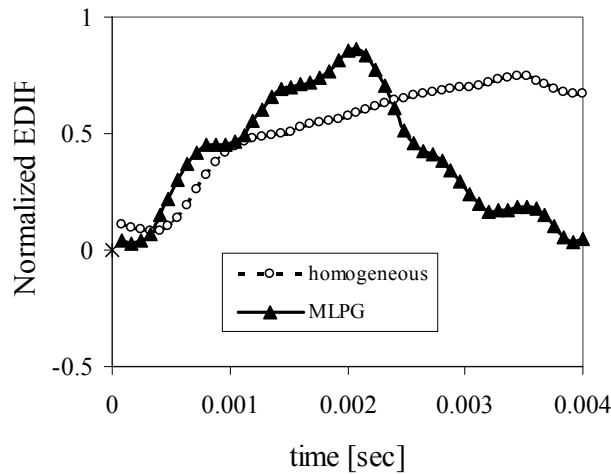


Figure 22: Temporal variations of the normalized EDIF for an edge crack in a homogeneous and FGPM strip with semi-permeable crack-face condition

6 Conclusions

A meshless local Petrov-Galerkin method (MLPG) is presented for 2-D crack problems in homogeneous and functionally graded piezoelectric materials. The linear MLPG solvers for the impermeable and permeable cracks are developed first and then an iterative procedure to reach the semi-permeable crack model is proposed. Energetically consistent boundary conditions on the crack-faces are considered too. This model is leading to consistency of total and crack-tip energy release rates. An additional closing traction is added to the well-known semi-permeable crack-face boundary conditions.

The governing partial differential equations are satisfied in a weak-form on small fictitious subdomains. A unit step function is used as the test function in the local weak-form of the governing partial differential equations on small circular subdomains spread on the analyzed domain. The moving least-squares (MLS) scheme is adopted for the approximation of the physical field quantities. The system of the ordinary differential equations of the second order resulting from the equations of motion is solved by the Houbolt finite-difference scheme as a time-stepping method. The proposed method is a truly meshless method, which requires neither domain elements nor background cells in either the interpolation or the integration. The results in several numerical examples show a strong coupling between the stress intensity factor and the electrical displacement intensity factor under the dy-

dynamic loadings although no coupling is observed for static loads. An impact load is leading to a dynamic overshoot of the static intensity factors. A gradation of the material properties affects both intensity factors.

The present method is an alternative numerical tool to many existing computational methods such as the FEM and the BEM. The main advantage of the present method is its simplicity. Compared to the conventional BEM, the present method requires no fundamental solutions and all integrands in the present formulation are regular. Thus, no special numerical techniques are required to evaluate the integrals. It should be noted here that the expressions of the fundamental solutions for piezoelectric materials with continuously varying properties are not available. The present formulation also possesses the generality of the FEM. Therefore, the method is promising for numerical analysis of multi-field problems.

Acknowledgement: The authors gratefully acknowledge the support by the Slovak Science and Technology Assistance Agency registered under number APVV-0427-07, the Slovak Grant Agency VEGA-2/0039/09, and the German Research Foundation (DFG, Project-No. ZH 15/6-3).

References

- Apte, D.A.; Ganguli, R.** (2009): Influence of Temperature and High Electric Field on Power Consumption by Piezoelectric Actuated Integrated Structure, *CMC: Computers, Materials, & Continua*, Vol. 10, No. 2, pp. 139-162?
- Atluri, S.N.** (2004): *The Meshless Method, (MLPG) For Domain & BIE Discretizations*, Tech Science Press.
- Atluri, S.N.; Han, Z.D.; Shen, S.** (2003): Meshless local Petrov-Galerkin (MLPG) approaches for solving the weakly-singular traction & displacement boundary integral equations. *CMES: Computer Modeling in Engineering & Sciences* 4, 507-516.
- Atluri, S.N.; Liu, H.T.; Han, Z.D.** (2006): Meshless local Petrov-Galerkin (MLPG) mixed finite difference method for solid mechanics. *CMES: Computer Modeling in Engineering & Sciences* 15, 1-16.
- Belytschko, T.; Krogauz, Y.; Organ, D.; Fleming, M.; Krysl, P.** (1996): Meshless methods; an overview and recent developments. *Comp. Meth. Appl. Mech. Engrn.* 139, 3-47.
- Chen, J.; Liu, Z.X.; Zou, Z.Z.** (2003): Electromechanical impact of a crack in a functionally graded piezoelectric medium. *Theoretical and Applied Fracture Mechanics* 39, 47-60.
- Davi, G.; Milazzo, A.** (2001): Multidomain boundary integral formulation for

piezoelectric materials fracture mechanics. *Int. J. Solids Structures* 38, 2557-2574.

Denda, M. (2008): BEM analysis of semipermeable piezoelectric cracks. *Key Engineering Materials* 383, 67-84.

Eischen, J.W. (1987): Fracture of nonhomogeneous materials. *International Journal of Fracture* 34, 3-22.

Enderlein, M.; Ricoeur, A.; Kuna, M. (2005): Finite element techniques for dynamic crack analysis in piezoelectrics. *International Journal of Fracture* 134, 191-208.

Fleming M.; Chu Y.A.; Moran B.; Belytschko T. (1997): Enriched element-free Galerkin methods for crack tip fields. *International Journal for Numerical Methods in Engineering* 40, 1483-1504.

Garcia-Sanchez, F.; Saez, A.; Dominguez, J. (2005): Anisotropic and piezoelectric materials fracture analysis by BEM. *Computers & Structures* 83, 804-820.

Garcia-Sanchez, F.; Zhang, Ch.; Sladek, J.; Sladek, V. (2007): 2-D transient dynamic crack analysis in piezoelectric solids by BEM. *Computational Materials Science* 39, 179-186.

Govorukha, V.; Kamlah, M. (2004): Asymptotic fields in the finite element analysis of electrically permeable interfacial cracks in piezoelectric bimetals. *Archive of Applied Mechanics* 74, 92-101.

Gruebner, O.; Kamlah, M.; Munz, D. (2003): Finite element analysis of cracks in piezoelectric materials taking into account the permittivity of the crack medium. *Eng. Fracture Mechanics* 70, 1399-1413.

Gross, D.; Rangelov, T.; Dineva, P. (2005): 2D wave scattering by a crack in a piezoelectric plane using traction BIEM. *SID: Structural Integrity & Durability* 1, 35-47.

Hao, T.H.; Shen, Z.Y. (1994): A new electric boundary condition of electric fracture mechanics and its applications. *Engineering Fracture Mechanics* 47, 793-802.

Houbolt J.C. (1950): A recurrence matrix solution for the dynamic response of elastic aircraft. *Journal of Aeronautical Sciences* 17, 371-376.

Jiang, A.; Wu, Y. (2009): The Boundary Contour Method for Piezoelectric Media with Quadratic Boundary Elements, *CMC: Computers, Materials, & Continua*, Vol. 12, No. 2, pp. 101-120

Jin, Z.H.; Noda, N. (1994): Crack-tip singular fields in nonhomogeneous materials. *ASME Journal of Applied Mechanics* 61, 738-740.

Kuna, M. (1998): Finite element analyses of crack problems in piezoelectric structures. *Computational Materials Science* 13, 67-80.

- Kuna, M.** (2006): Finite element analyses of cracks in piezoelectric structures – a survey. *Archive of Applied Mechanics* 76, 725-745.
- Landis, C.M.** (2004): Energetically consistent boundary conditions for electromechanical fracture. *Int. J. Solids Structures* 41, 6291-6315.
- Li, C.; Weng, G.J.** (2002): Antiplane crack problem on functionally graded piezoelectric materials. *ASME Journal of Applied Mechanics* 69, 481-488.
- Liu, G.R.; Dai, K.Y.; Lim, K.M.; Gu, Y.T.** (2002): A point interpolation mesh free method for static and frequency analysis of two-dimensional piezoelectric structures. *Computational Mechanics* 29, 510-519.
- McMeeking, R.M.** (1999): Crack tip energy release rate for a piezoelectric compact tension specimen. *Engineering Fracture Mechanics* 64, 217-244.
- McMeeking, R.M.** (2004): The energy release rate for a Griffith crack in a piezoelectric material. *Engineering Fracture Mechanics* 71, 1149-1163.
- Ohs, R.R.; Aluru, N.R.** (2001): Meshless analysis of piezoelectric devices. *Computational Mechanics* 27, 23-36.
- Pan, E.** (1999): A BEM analysis of fracture mechanics in 2D anisotropic piezoelectric solids. *Engineering Analysis with Boundary Elements* 23, 67-76.
- Pak, Y.E.** (1990): Crack extension force in a piezoelectric material. *ASME J. Applied Mechanics* 57, 647-653.
- Pak, Y.E.** (1992): Linear electro-elastic fracture mechanics of piezoelectric materials. *International Journal of Fracture* 54, 79-100.
- Park, S.B.; Sun, C.T.** (1995): Effect of electric field on fracture of piezoelectric ceramics. *International Journal of Fracture* 70, 203-216.
- Parton, V.Z.; Kudryavtsev, B.A.** (1988): *Electromagnetoelasticity, Piezoelectrics and Electrically Conductive Solids*. Gordon and Breach Science Publishers, New York.
- Paulino, G.H.; Jin, Z.H.; Dodds, R.H.** (2003): *Failure of functionally graded materials*. In: Karihaloo B, Knauss WG, editors, *Comprehensive Structural Integrity*, Volume 2, Elsevier Science, 607-644.
- Sheng, N.; Sze, K.Y.** (2006): Multi-region Trefftz boundary element method for fracture analysis in plane piezoelectricity. *Computational Mechanics* 37, 381-393.
- Sladek, J.; Sladek, V.; Atluri, S.N.** (2004): Meshless local Petrov-Galerkin method in anisotropic elasticity. *CMES: Computer Modeling in Engn. & Sciences* 6, 477-489.
- Sladek, J.; Sladek, V.; Zhang, Ch.; Garcia-Sanchez, F.; Wünsche, M.** (2006): Meshless Local Petrov-Galerkin Method for Plane Piezoelectricity. *CMC: Com-*

puters, Materials & Continua 4, 109-118.

Sladek, J.; Sladek, V.; Zhang, Ch.; Solek, P.; Starek, L. (2007a): Fracture analyses in continuously nonhomogeneous piezoelectric solids by the MLPG. *CMES: Computer Modeling in Engn. & Sciences* 19, 247-262.

Sladek J.; Sladek V.; Zhang Ch.; Solek P.; Pan E. (2007b): Evaluation of fracture parameters in continuously nonhomogeneous piezoelectric solids. *Int. J. Fracture* 145, 313–326.

Sosa, H. (1991): Plane problems in piezoelectric media with defects. *Int. J. Solids Structures* 28, 491-505.

Suo, Z.; Kuo, C.M.; Barnett, D.M.; Willis, J.R. (1992): Fracture mechanics for piezoelectric ceramics. *Journal of Mechanics and Physics of Solids* 4, 739-765.

Suresh, S.; Mortensen, A. (1998): *Fundamentals of Functionally Graded Materials*. Institute of Materials, London.

Ueda, S. (2003): Crack in functionally graded piezoelectric strip bonded to elastic surface layers under electromechanical loading. *Theoretical Applied Fracture Mechanics* 40, 225-236.

Wang, B.L.; Noda, N. (2001): Thermally induced fracture of a smart functionally graded composite structure. *Theoretical Applied Fracture Mechanics* 35, 93-109.

Wen P.H.; Aliabadi M.H. (2007): Meshless method with enriched radial basis functions for fracture mechanics. *Structural Durability & Health Monitoring* 3, 107-119.

Wen P.H.; Aliabadi M.H. (2008): An improved meshless collocation method for elastostatic and elastodynamic problems. *Communications in Numerical Methods in Engineering* 24, 635-651.

Wen P.H.; Aliabadi M.H.; Liu Y.W. (2008): Meshless method for crack analysis in functionally graded materials with enriched radial base functions. *CMES: Computer Modeling in Engineering & Sciences* 30, 133–147.

Wünsche, M.; Garcia-Sanchez, F.; Saez, A.; Zhang, Ch. (2010): A 2D time domain collocation-Galerkin BEM for dynamic crack analysis in piezoelectric solids. *Engineering Analysis with Boundary Elements* 34, 377-387.

Zhu, T.; Zhang, J.D.; Atluri, S.N. (1998): A local boundary integral equation (LBIE) method in computational mechanics, and a meshless discretization approaches. *Computational Mechanics* 21, 223-235.

Zhu, X.; Wang, Z.; Meng, A. (1995): A functionally gradient piezoelectric actuator prepared by metallurgical process in PMN-PZ-PT system. *J. Mater. Sci Lett.* 14, 516-518.

Zhu, X.; Zhu, J.; Zhou, S.; Li, Q.; Liu, Z. (1999): Microstructures of the monomorph piezoelectric ceramic actuators with functionally gradient. *Sensors Actuators A* 74, 198-202.

